Received 17 September 2020; revised 27 October 2020; accepted 29 November 2020. Date of publication 2 December 2020;
date of current version 28 January 2021. The review of this article was arranged by Editor P. Pavan

Digital Object Identifier 10.1109/JEDS.2020.3042050

First RF Power Operation of AlN/GaN/AlN HEMTs With >3 A/mm and 3 W/mm at 10 GHz

AUSTIN HICKMAN[1] (Graduate Student Member, IEEE), REET CHAUDHURI[1] (Graduate Student Member, IEEE), LEI LI[1] (Graduate Student Member, IEEE), KAZUKI NOMOTO[1] (Member, IEEE), SAMUEL JAMES BADER[2] (Member, IEEE), JAMES C. M. HWANG[3] (Life Fellow, IEEE), HUILI GRACE XING[1,3] (Senior Member, IEEE), AND DEBDEEP JENA[1,2,3] (Senior Member, IEEE)

1 Department of Electrical and Computer Engineering, Cornell University, Ithaca, NY 14853, USA
2 Applied and Engineering Physics Department, Cornell University, Ithaca, NY 14853, USA
3 Material Science and Engineering Department, Cornell University, Ithaca, NY 14853, USA

CORRESPONDING AUTHOR: A. HICKMAN (e-mail: alh288@cornell.edu)

This work was supported in part by Semiconductor Research Corporation Joint University Microelectronics Program; in part by the AFOSR under Grant FA9550-17-1-0048; and in part by NSF DMR under Grant 1710298.

ABSTRACT The AlN/GaN/AlN heterostructure is attractive for microwave and millimeter-wave power devices due to its thin top barrier, tight carrier confinement, and improved breakdown voltage. This work explores the large-signal RF performance of high-electron-mobility transistors on this heterostructure. Results are highlighted by record high on-current of 3.6 A/mm, and record maximum oscillation frequency (f_{max}) of 233 GHz. The load-pull power sweep at 10 GHz demonstrate a peak power added efficiency (PAE) of 22.7% with an associated gain (G_T) of 8.7 dB and output power (P_{out}) of 3 W/mm. When optimized for power, the peak P_{out} of 3.3 W/mm has an associated PAE of 14.7% and G_T of 3.2 dB. This first demonstration is encouraging for the mm-wave power potential of the AlN/GaN/AlN HEMT.

INDEX TERMS GaN, AlN, output power, mm-wave, load-pull.

I. INTRODUCTION

The demand for millimeter-wave (mm-wave) power amplifiers continues to grow for next-generation cellular communication networks and defense radar applications. Gallium nitride high-electron-mobility transistors (GaN HEMTs), with high breakdown voltage and high electron saturation velocity, are a premier platform for the future of mm-wave solid-state power amplification [1]. The conventional GaN HEMT consists of an AlGaN/GaN heterostructure. Previous demonstrations of AlGaN/GaN HEMT output power with field plating have shown over 40 W/mm at 4 GHz [2], 30.6 W/mm at 8 GHz [3] and up to 13.7 and 10 W/mm at 30 GHz [4], [5]. By significantly enhancing device breakdown, field plates also increase output power, but due to the complexity of properly implementing field plates in highly-scaled RF devices [6], it can be valuable, for the purpose of evaluating the potential for a new heterostructure, to compare devices without field-shaping. Without field plates, the AlGaN/GaN and other heterostructures have been assessed, with AlGaN/GaN HEMTs showing 10.5 W/mm at 40 GHz [7], AlN/GaN HEMTs demonstrating 4 W/mm at 94 GHz [8], and InAlGaN barrier HEMTs showing 3 W/mm at 96 GHz [9]. Most notably, N-polar GaN HEMTs have demonstrated over 8 W/mm at the range of 10 to 94 GHz [10]–[12]. Across all current non-field-plated GaN HEMTs technologies, device breakdown voltage plays a limiting role in the maximum output power.

To further increase the HEMT breakdown voltage while improving mm-wave performance, the AlN/GaN/AlN HEMT was proposed [13]. The heterostructure consists of a GaN channel between a relaxed AlN buffer and an AlN top barrier. The transition to a majority AlN structure offers both material and device advantages over the conventional heterostructure: the AlN buffer tightly confines the 2DEG and offers a higher thermal conductivity path than a thick GaN buffer, and the AlN barrier induces a higher density

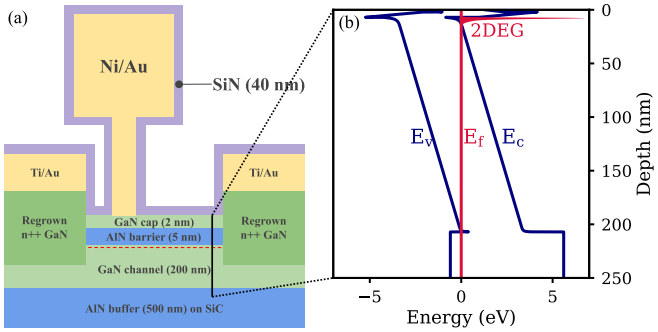

FIGURE 1. (a) Cross-sectional representation of a fully processed AlN/GaN/AlN HEMT with a shifted T-gate. (b) 1D-Poisson simulation of the heterostructure band diagram. Readers interested in the two-dimensional hole gas, not indicated, at the channel/buffer interface may see [16].

two-dimensional electron gas (2DEG) closer to the gate (5 nm) for more effective channel modulation. AlN also maximizes the barrier bandgap, improving the breakdown voltage. Additionally, the AlN buffer offers a promising platform for p-channel FETs, enabling the possibility for all-nitride CMOS [14]–[16].

Since proposed, AlN/GaN/AlN HEMTs have shown high on-currents at 2.8 A/mm, and small-signal measurements for rectangular gate devices yielded a cutoff frequency (f_t) of 120 GHz [17]. Most recently, the breakdown voltage of AlN/GaN/AlN HEMTs was assessed, with devices demonstrating breakdown fields above 2 MV/cm, and a Johnson figure of merit ($f_t \times V_{D,f_t}$) of 2 THz·V [18]. However, all previous iterations of HEMTs were not assessed for output power due the rectangular gate geometry and associated high gate resistance. In this letter, a T-gate geometry was incorporated on the AlN/GaN/AlN devices and output power assessment was performed for the first time.

II. EPITAXIAL GROWTH AND DEVICE FABRICATION

The AlN/GaN/AlN heterostructure measured in this report was grown by plasma-assisted Molecular Beam Epitaxy (MBE) on highly resistive 6H silicon carbide. The heterostructure is composed of a 500 nm AlN buffer layer, a 200 nm GaN channel, a 5 nm AlN barrier, and a 2 nm GaN passivation layer, as shown in Fig. 1(a). Hall-effect measurements in Van der Pauw configuration were performed on the as-grown heterostructure, demonstrating a room temperature 2DEG concentration of $3 \cdot 10^{13}$ cm^{-2} and electron mobility of 723 cm^2/V·s, resulting in a sheet resistance of 293 Ω/sq. This measured mobility is close to the highest mobilities reported in the AlN/GaN/AlN structure of around 750 cm^2/V·s [17]–[22]. To study the observed mobility limitations and the potential effect of the 2-dimensional hole gas (2DHG) that forms at the GaN channel/AlN buffer interface, the GaN channel for the heterostructure in this report was increased from 30 nm [18] in thickness to 200 nm. This mobility study is ongoing, but is not the focus of this report. The longer term goal for this heterostructure is to scale down the GaN channel thickness while achieving 2DEG mobilities comparable to those in state-of-the-art AlGaN/GaN heterostructures (> 1500 cm^2/V·s). Doing this will take full advantage of what AlN offers without sacrificing carrier mobility.

Device fabrication began with the regrown ohmic contact process. The as-grown heterostructure was masked with SiO_2/Chromium, patterned for source/drain contacts, and dry-etched by chlorine-based inductively-coupled plasma (ICP) to expose the 2DEG sidewall. The sample was then loaded into the MBE chamber, and n++ GaN ([Si] ~ 10^{20}cm^{-3}) was grown to form ohmic contacts to the 2DEG. The devices were isolated by another chlorine-based ICP etch, and Ti/Au (50/100 nm) ohmic metals were deposited via e-beam evaporation on top of the regrown GaN without annealing. The T-gate contacts were formed using a tri-layer resist stack, and a single electron beam lithography (EBL) exposure. The Ni/Au (50/200 nm) T-gate metals were deposited by e-beam evaporation. The T-gates were aligned to the regrown GaN, and offset towards the source contact (L_{GS} = 200 nm) to enhance device breakdown. The HEMTs were passivated with 40 nm of plasma-enhanced chemical vapor deposition silicon nitride (PECVD SiN). The passivation was removed on the gate, drain, and source probe pads, which were then thickened with an additional Ti/Au (50/300 nm) layer via e-beam evaporation. Fig. 1(a) shows a representative cross section of the fully processed HEMT and Fig. 2(d) shows a scanning electron microscope (SEM) image of the T-gates.

III. EXPERIMENTAL RESULTS AND DISCUSSION

The contact resistance was measured via transfer-length-method (TLM) test structures, which include the metal contacts to regrown GaN resistance, as well the regrown GaN to 2DEG resistance. The total contact resistance was 0.15 Ω·mm. All measured HEMTs are 2×25 μm in width. DC current-voltage transfer measurements (Fig. 2(a)) showed a threshold voltage of −4 V, a peak transconductance (g_m) of 0.6 S/mm, and an on/off ratio of 3×10^2 (this value was 10^6 prior to SiN passivation). The reduction in on/off ratio is due to an increase in the off-state gate leakage current. A potential cause is surface leakage paths, both on the surface of the active area and on the exposed GaN in the isolation region, that are enhanced by SiN deposition. This issue will be addressed in future devices with isolation via ion implantation and epitaxial passivation. Output measurements revealed a typical on-resistance of 1Ω·mm, and drain currents above 3 A/mm for nearly all HEMTs measured, with the highest drain current (I_D) of 3.6 A/mm (Fig. 2(c)) for V_G, V_D = 3, 10 V, a record for devices on the majority-AlN heterostructure.

Drain-induced barrier lowering (DIBL) was assessed for three HEMTs with varied L_{DS} (0.6, 0.8, 1 μm) and L_G (50, 60, 90 nm). The shift in gate voltage was measured at I_D = 150 mA/mm for a drain bias ranging from 2 to 20 V. All three HEMTs showed a DIBL of 17 mV/V or less. This is among the lowest reported DIBL values for GaN

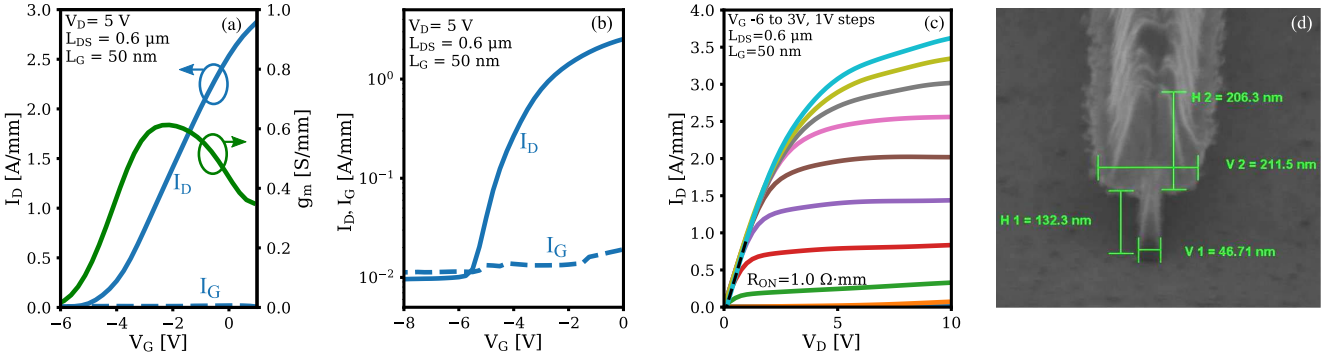

FIGURE 2. The (a) linear and (b) log transfer characteristics for a AlN/GaN/AlN HEMT showing $g_m = 0.6$ S/mm. The (c) output measurements demonstrate a record $I_D = 3.6$ A/mm. (d) SEM image of a T-gate with $L_G < 50$ nm.

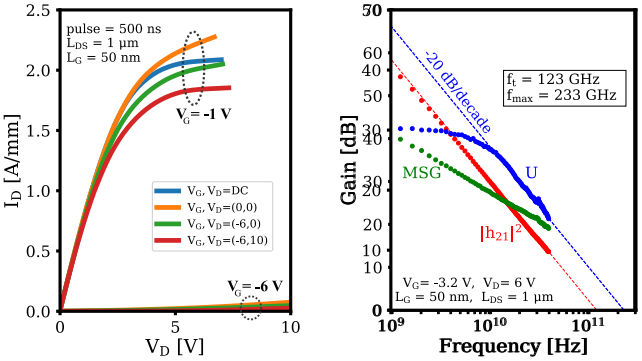

FIGURE 3. (a) Pulsed I_D-V_D measurements for a 500 ns pulse, at a bias of $V_G = -6$ V and -1 V. A 20% dispersion in the saturation region and ~1 V knee voltage walkout is observed at 10 V drain lag conditions. (b) The small-signal characteristics for a HEMT with $L_G = 50$ nm, with a resulting $f_t/f_{max} = 123/233$ GHz.

HEMTs [23], [24], and it is indicative of the strong carrier confinement expected in the AlN/GaN/AlN heterostructure.

Pulsed $I_D - V_{DS}$ measurements were performed after SiN passivation using a 500 ns pulse and 0.05% duty cycle. The device demonstrated an on-current dispersion of 20% and ~1 V knee voltage walkout for quiescent gate/drain biases of $-6/10$ V, as shown in Fig. 3(a). Bias-dependent S-parameters were then measured in the range of 0.05-40 GHz. The system was de-embedded via a short-open-load-through impedance standard substrate and on-wafer open/short structures. The device measured for dispersion also demonstrated $f_t = 123$ GHz, $f_{max} = 233$ GHz, at a bias of V_G, $V_D = -3.2, 6$ V for maximum transconductance, as shown in Fig. 3(b). This is the highest f_{max} reported for devices on the AlN/GaN/AlN heterostructure, and can be attributed to the incorporation of the T-gate geometry.

Large-signal performance was evaluated using a Maury load-pull system at 10 GHz. For a device with $L_G = 50$ nm, $L_{DS} = 2$ μm, and $L_{GD} = 1.5$ μm, the optimum source ($\Gamma_S = 0.68 + j0.30$) and load ($\Gamma_L = 0.70 + j0.14$) reflection coefficients were tuned for maximum PAE, with the maximum gamma for the load pull system being 0.85. The device was biased in Class AB conditions, with an I_{DSq} of 470 mA/mm and V_{DSq} of 20 V. Fig. 4(a) shows the power sweep results for the device, demonstrating a peak P_{out} of 22.2 dBm, equivalent to 3.3 W/mm, with an associated PAE of 14.7%, drain efficiency of 36.6%, and G_T of 3.2 dB. The peak PAE of 22.7% had an associated P_{out} of 3 W/mm and G_T of 8.7 dB. To validate the large signal measurements, the measured gain of 16.2 dB at Pin = 1 dBm (1 dBm being the lower limit of the measurement range) is compared to the small-signal maximum stable gain (MSG) of 20 dB at 10 GHz for the same HEMT. The 3.8 dB difference is attributed to the parasitics of the metal pads (measured 1.2 dB), the device being load line matched rather than conjugate matched, the difference in bias points, and the combination of current collapse and knee voltage walkout.

The saturated output power of 3.3 W/mm is hampered by the soft gain compression, which becomes limiting as the input power increases. This is likely caused by surface traps and back gating from charge trapping at the AlN/SiC interface [25], [26]. This is also supported in Fig. 4(b), where the G_T and PAE of the device decrease for an increasing V_{DSq}. To reduce the effects of dispersion in future devices, a passivation-first or in-situ passivation process will be incorporated.

IV. CONCLUSION

In this letter, the large-signal operation of AlN/GaN/AlN HEMTs was explored for the first time. The devices demonstrated on-current and f_{max} records of 3.6 A/mm and 233 GHz, respectively, for HEMTs on the AlN platform. Load-pull power sweep measurements demonstrated a peak output power of 3.3 W/mm at 10 GHz, with a PAE of 14.7% and gain (G_T) of 3.2 dB. This encouraging data provides a clear path for improved output power via an optimized passivation process, and serves as critical first step for the establishment of AlN as a platform for the next generation of mm-wave solid-state power devices.

ACKNOWLEDGMENT

The work was performed at Cornell NanoScale Facility (NNCI member supported by NSF ECCS-1542081), and

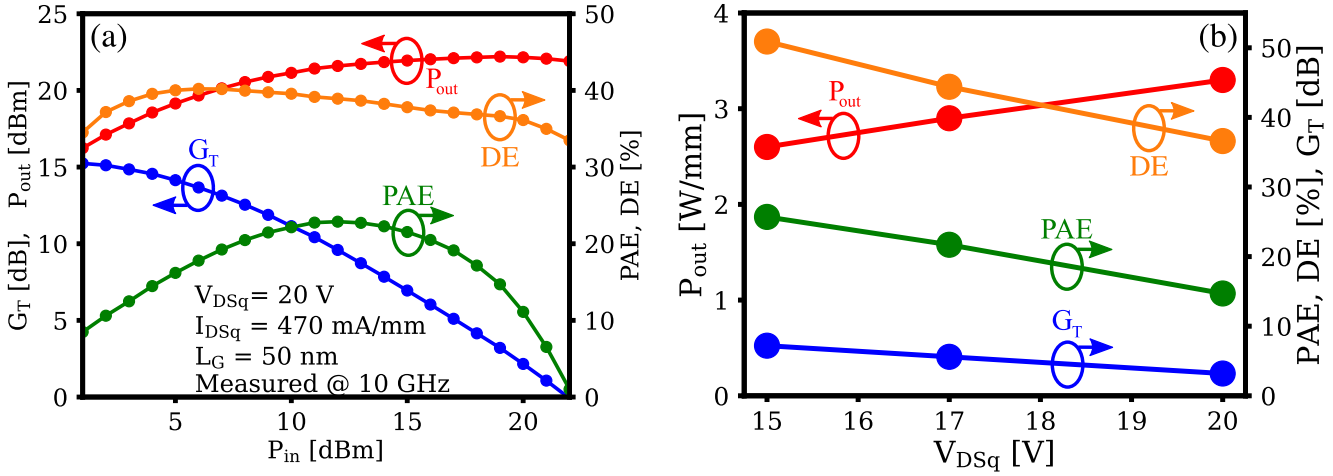

FIGURE 4. **(a) Load-pull power sweep at 10 GHz for a 2 × 25 μm device biased in Class AB operation ($V_{DSq} = 20V$, $I_{DSq} = 470$ mA/mm). (b) Output power, gain, drain efficiency (DE), and PAE are given for the device at V_{DSq} values of 15, 17, and 20 V.**

Cornell Center for Materials Research, supported by NSF MRSEC DMR-1719875.

REFERENCES

[1] Y.-K. Chen, T.-H. Chang, and A. Sivananthan, "Advanced mm-wave power electronics (invited talk)," in *Proc. IEEE BiCMOS Compound Semicond. Integr. Circuits Technol. Symp. (BCICTS)*, 2019, pp. 1–4.

[2] Y.-F. Wu, M. Moore, A. Saxler, T. Wisleder, and P. Parikh, "40-W/mm double field-plated GaN HEMTs improvements," in *Device Res. Conf. Dig. (DRC)*, 2006, pp. 151–152.

[3] Y.-F. Wu *et al.*, "30-W/mm GaN HEMTs by field plate optimization," *IEEE Electron Device Lett.*, vol. 25, no. 3, pp. 117–119, Mar. 2004.

[4] Y.-F. Wu *et al.*, "High-voltage millimeter-wave GaN HEMTs with 13.7 W/mm power density," in *Proc. IEEE Int. Electron Devices Meeting*, 2007, pp. 405–407.

[5] J. S. Moon *et al.*, "55% PAE and high power Ka-band GaN HEMTs with linearized transconductance via n+ GaN source contact ledge," *IEEE Electron Device Lett.*, vol. 29, no. 8, pp. 834–837, Aug. 2008.

[6] P. Fay, D. Jena, and P. Maki, *High-Frequency GaN Electronic Devices*. Cham, Switzerland: Springer, 2020, pp. 83–107. [Online]. Available: https://doi.org/10.1007/978-3-030-20208-8_4

[7] T. Palacios *et al.*, "High-power AlGaN/GaN HEMTs for Ka-band applications," *IEEE Electron Device Lett.*, vol. 26, no. 11, pp. 781–783, Nov. 2005.

[8] K. Harrouche, R. Kabouche, E. Okada, and F. Medjdoub, "High performance and highly robust AlN/GaN HEMTs for millimeter-wave operation," *IEEE J. Electron Devices Soc.*, vol. 7, pp. 1145–1150, 2019.

[9] K. Makiyama *et al.*, "Collapse-free high power InAlGaN/GaN-HEMT with 3 W/mm at 96 GHz," in *Tech. Dig. Int. Electron Devices Meeting (IEDM)*, vol. 2016, Feb. 2015, pp. 9.1.1–9.1.4.

[10] B. Romanczyk *et al.*, "Record 34.2% efficient mm-wave N-Polar AlGaN/GaN MISHEMT at 87 GHz," *Electron. Lett.*, vol. 52, no. 21, pp. 1813–1814, Oct. 2016.

[11] B. Romanczyk *et al.*, "Demonstration of constant 8 W/mm power density at 10, 30, and 94 GHz in state-of-the-art millimeter-wave N-polar GaN MISHEMTs," *IEEE Trans. Electron Devices*, vol. 65, no. 1, pp. 45–50, Jan. 2018.

[12] B. Romanczyk *et al.*, "W-band power performance of SiN-passivated N-polar GaN deep recess HEMTs," *IEEE Electron Device Lett.*, vol. 41, no. 3, pp. 349–352, Mar. 2020.

[13] G. Li *et al.*, "Ultrathin body GaN-on-insulator quantum well FETs with regrown Ohmic contacts," *IEEE Electron Device Lett.*, vol. 33, no. 5, pp. 661–663, May 2012.

[14] S. J. Bader *et al.*, "Gate-recessed E-mode p-channel HFET with high on-current based on GaN/AlN 2D hole gas," *IEEE Electron Device Lett.*, vol. 39, no. 12, pp. 1848–1851, Dec. 2018.

[15] S. J. Bader *et al.*, "GaN/AlN Schottky-gate p-channel HFETs with InGaN contacts and 100 mA/mm on-current," in *Tech. Dig. Int. Electron Devices Meeting (IEDM)*, Dec. 2019, pp. 4.5.1–4.5.4.

[16] R. Chaudhuri, S. J. Bader, Z. Chen, D. A. Muller, H. G. Xing, and D. Jena, "A polarization-induced 2D hole gas in undoped gallium nitride quantum wells," *Science*, vol. 365, no. 6460, pp. 1454–1457, 2019.

[17] M. Qi *et al.*, "Strained GaN quantum-well FETs on single crystal bulk AlN substrates," *Appl. Phys. Lett.*, vol. 110, no. 6, 2017, Art. no. 063501. [Online]. Available: http://dx.doi.org/10.1063/1.4975702

[18] A. Hickman *et al.*, "High breakdown voltage in RF AlN/GaN/AlN quantum well HEMTs," *IEEE Electron Device Lett.*, vol. 40, no. 8, pp. 1293–1296, Aug. 2019.

[19] G. Li *et al.*, "Two-dimensional electron gases in strained quantum wells for AlN/GaN/AlN double heterostructure field-effect transistors on AlN," *Appl. Phys. Lett.*, vol. 104, no. 19, 2014, Art. no. 193506. [Online]. Available: http://dx.doi.org/10.1063/1.4875916

[20] S. Rennesson *et al.*, "Ultrathin AlN-based HEMTs grown on silicon substrate by NH3-MBE," *Physica Status Solidi A, Appl. Mater. Sci.*, vol. 215, no. 9, 2018, Art. no. 1700640.

[21] G. Doundoulakis *et al.*, "Experimental and modeling insight for fin-shaped transistors based on AlN/GaN/AlN double barrier heterostructure," *Solid-State Electron.*, vol. 158, pp. 1–10, Aug. 2019. [Online]. Available: https://doi.org/10.1016/j.sse.2019.04.005

[22] S. Patwal, M. Agrawal, K. Radhakrishnan, T. L. A. Seah, and N. Dharmarasu, "Enhancement of 2D electron gas mobility in an AlN/GaN/AlN double-heterojunction high-electron-mobility transistor by epilayer stress engineering," *Physica Status Solidi A, Appl. Mater. Sci.*, vol. 217, no. 7, Apr. 2020, Art. no. 1900818.

[23] D. S. Lee, X. Gao, S. Guo, and T. Palacios, "InAlN/GaN HEMTs with AlGaN back barriers," *IEEE Electron Device Lett.*, vol. 32, no. 5, pp. 617–619, May 2011. [Online]. Available: http://ieeexplore.ieee.org/document/5723687/

[24] X. Zheng *et al.*, "High frequency N-polar GaN planar MIS-HEMTs on sapphire with high breakdown and low dispersion," in *Proc. 25th Biennial Lester Eastman Conf. (LEC)*, 2016, pp. 42–45.

[25] J. C. Pedro, L. C. Nunes, and P. M. Cabral, "Soft compression and the origins of nonlinear behavior of GaN HEMTs," in *Proc. 44th Eur. Microw. Integr. Circuit Conf.*, 2014, pp. 1297–1300.

[26] J. C. M. Hwang, "Relationship between gate lag, power drift, and power slump of pseudomorphic high electron mobility transistors," *Solid-State Electron.*, vol. 43, no. 8, pp. 1325–1331, 1999.